Selective Detection of Protein Crystals by Second Harmonic Microscopy

Ronald D. Wampler, David J. Kissick, Christopher J. Dehen, Ellen J. Gualtieri,
Jessica L. Grey, Hai-Feng Wang[†], David H. Thompson, Ji-Xin Cheng[†], Garth J. Simpson[*]

Department of Chemistry and Biomedical Engineering[†], Purdue University, West Lafayette, IN 47906.

Supporting Information

This section includes detailed information on; 1) assessment of the minimum detectable chiral crystal size by SHG microscopy, 2) discussion of the nature of the image contrast observed in SHG measurements of lysozyme crystals, 3) description of the instrumentation, 4) methods for the expression, purification and crystallization of GFP, and 5) methods for the crystallization of lysozyme.

I. Crystal Size Detection Limit Determination using (L)-lysine

The minimum crystal size detected by SHG was estimated by monitoring the transmitted and epi-detected SHG generated during crystallization of lysine by slow evaporation. For a particle thickness much less than the wavelength of light, the efficiency of generating forward versus backward propagating SHG is nearly equal. However, when the physical thickness of the SHG-active crystals generated upon evaporation reach a thickness approaching roughly $\lambda/2$, the ratio of forward to backward generated SHG transitions to predominantly forward scattering.[1] Consequently, the transition point at which the ratio of the F/B ratio departs from a value of ~1 serves as a built-in "ruler" for estimation of the particle size. The signal to noise ratio (S/N) of ~9 at this transition point corresponds to a particle with a diameter of ~200 nm. Assuming that the signal scales with the volume of monomers within the crystal lattice for a spherical particle and Poisson noise and including contributions from dark counts, the cubic dependence of the signal on volume puts the minimum detection size for this configuration at ~100 nm for a S/N of 3. This estimate for the detection limit is approximately 1/20 the beam waist used in the measurements.

II. SHG Microscopy of Lysozyme Crystals

SHG microscopy measurements of lysozyme crystals are particularly interesting. In an initially paradoxical trend, the regions of high image contrast in SHG microscopy measurements of lysozyme crystals consisted primarily of polycrystalline conglomerates and small optical scattering centers within the lysozyme lattice (presumably attributable to lattice defects). Relatively large, pristine crystals generated much weaker SHG-activity. Three effects were considered for influencing the overall strength of the SH response arising from lysozyme crystals: i) the inherit SH activity of the protein crystals itself; ii) the angle of incidence of the laser probe relatively to the crystallographic axes; iii) the interplay between the size of the crystals and the geometry used to collect the SH signals [i.e., the forward or backwards (epi) direction].

The net NLO tensor for crystalline lysozyme was estimated by using NLOPredict in combination with quantum chemical calculations of the amide chromophores. NLOPredict is a program designed in part to predict the net tensors of proteins and protein crystals through orientational averaging of the different chromophores inherent in the protein structure (e.g., amide units).[2] The known structure for the $P4_32_12$ polymorph expected under these experimental conditions was used in the predictions along with the non-resonant tensor for the amide monomer, calculated by a double sum-over-states approach including 100 excited states to achieve convergence. It was assumed in the calculations that the amide chromophores dominate the net NLO response of lysozyme by nature of their relatively high number density. Including contributions from the aromatic side-chains may increase the net SHG activity predicted for lysozyme. Based on this approach, orientational averaging associated with the symmetry operations of the crystal significantly reduces the net NLO activity of lysozyme crystals. The squared norm (i.e., the sum of the squares of each tensor element) of a lysozyme monomer is approximately 154 times that of a single amide monomer, but the symmetry operations of the lattice reduce the net contributions per lysozyme to just 1.3 times that of a single amide monomer. This high degree of cancellation arises primarily by the presence of the 4-fold screw axis combined with the orthogonal 2-fold screw axis, collectively leaving only the Kleinman-disallowed chiral contributions remaining.[3-5] Inspection of the contents within the protein crystallographic data bank suggests that ~95% of protein crystals fall into symmetry classes that do not contain a 4-fold or higher rotational axis, such that the net SHG activities of most protein systems can be reasonably expected to far exceed those of this lysozyme polymorph.

For relatively large crystals with thicknesses much greater than the wavelength of light, the SHG can be reasonably expected to arise predominantly in the forward-scattering direction.[1] This expectation was consistent with measurements of lysozyme crystals

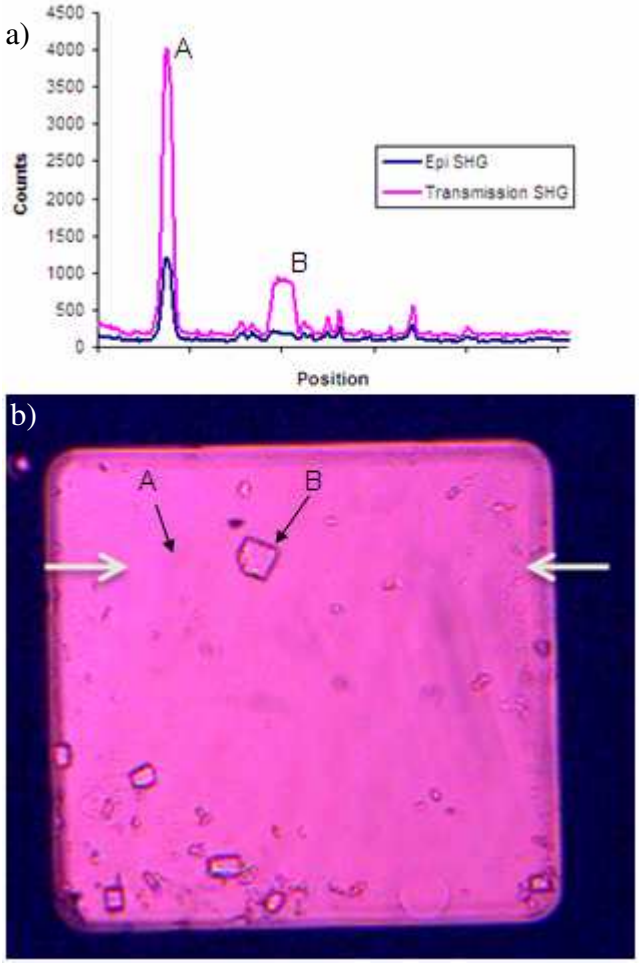

Figure S1. Brightfield (b) and corresponding line scan (a) of lysozyme crystals grown in ~1nl sealed well.

acquired in both epi and transmission, shown in Figure S1. The SHG line scan in Figure S1 contains two major features, a narrow peak which appears in both epi and transmission and a broad peak solely in transmission. The first peak (A) corresponds to a crystal that is not visible in the brightfield, whereas the second peak (B) is easily visible.

The preference toward forward-propagating SHG in large macroscopic crystals is also consistent with the relatively weak signals observed in the imaging measurements of lysozyme crystals shown in Figure S2. In the epi-detection configuration used, the relatively small microcrystals produces strong signals, while the large (>100 μm) bulk crystals were only weakly active.

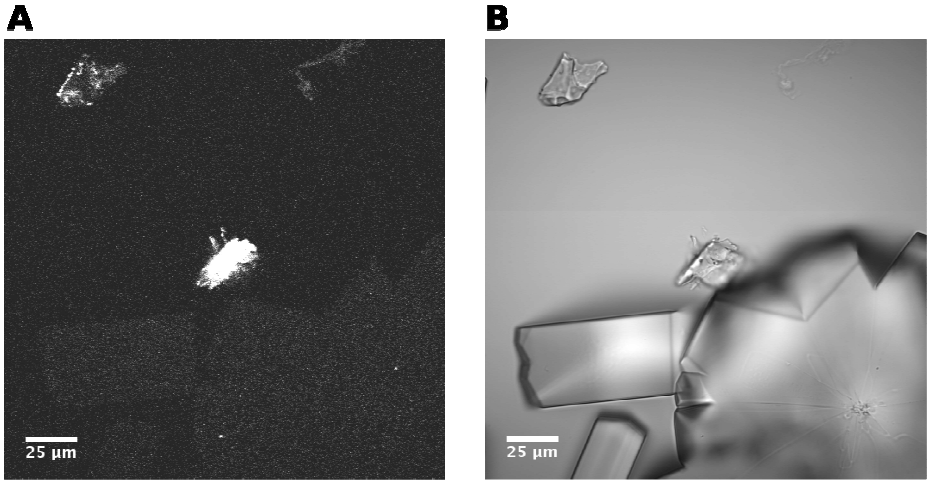

Figure S2. SHG micrograph (A) and corresponding bright field image (B) of lysozyme crystals.

Finally, the surface itself likely played a role in orienting the lysozyme crystals relative to the direction of propagation of the beam. All microscopy measurements were performed with the k-vector of the beam incident normal to the glass surface upon which the lysozyme crystals were grown. Because the only symmetry-allowed nonzero elements for this polymorph of lysozyme are $\chi_{XYZ} = \chi_{XZY} = -\chi_{YXZ} = -\chi_{YZX}$, no SHG can arise if the beam is propagating directly along a crystallographic axis. This argument is consistent with the measurements shown in Figure 2 of the primary manuscript, in which similarly prepared lysozyme crystals generate much stronger SHG-activity when the substrate plane is tilted relative to the beam propagation axis.

The intrinsically low SHG activity of lysozyme coupled with the use of epi-detection in a direction likely along a crystallographic axis collectively explain the relatively weak responses observed for the larger lysozyme crystals. These same explanations are also consistent with the observed maxima in SHG in the lysozyme micrographs from polycrystalline conglomerates and from defects within the lysozyme lattice. In both cases, the factors that conspired to reduce the SHG activity of macroscopic crystals are relaxed. Polycrystalline domains are more likely to be relatively small and therefore efficient generators in the epi-detection configuration. Furthermore, the absence of surface templating allows the crystalline domains to adopt more favorable orientations relative to the beam axis.

III. Instrumentation.

SHG images of lysozyme were obtained using several systems. Transmission measurements at angle of incidence of 0° and 45° were performed using nanosecond pulses (1 mJ/pulse) of 1064 nm light from a Nd:YAG laser with a 20Hz repetition rate. The incident light was *p*-polarized. Lysozyme crystals shown in Figure 2 of the manuscript were imaged using a mode-locked Ti:Sapphire laser (Mai Tai, Spectra Physics) at 840 nm with a pulse width of 130 fs and a repetition rate of 77 MHz. The power was 50 mW. The laser beam was directed into a laser scanning confocal microscope (FV1000, Olympus Inc.) with a 60X water-immersion objective (NA = 1.2).

The SHG and TPEF images of GFP crystals shown in Figure 1 were acquired by a combination of beam scanning and sampling scanning (Figure S3). An 80 MHz mode-locked Ti:Sapphire (Kapteyn-Murnane Labs) laser was directed into a Nikon eclipse TE-2000U microscope and focused by an 10x objective (NA= 0.3) onto the sample. The laser pulses were 40 fs with 50 mW average power at the sample. The beam was scanned along the fast scan axis by a resonant vibrating mirror at 7.8027 kHz and the samples were translated along the slow scan axis by an automated translation stage (Newport). A 400 nm dichroic mirror directed the epi-SHG through a filter stack (ir-blocking + 400 nm interference filter) toward a photomultiplier tube (PMT). The rest of the light was directed toward a PMT with a ir blocking filters and a 532 nm interference filter to collect the epi-TPEF. The transmitted SHG was collected through a 10x objective (NA = 0.25) and directed toward a PMT using a similar set of filters as in the epi-detection configuration. The line scans were compiled into an 8-bit grayscale image, which was digitally adjusted to overlay with the brightfield image.

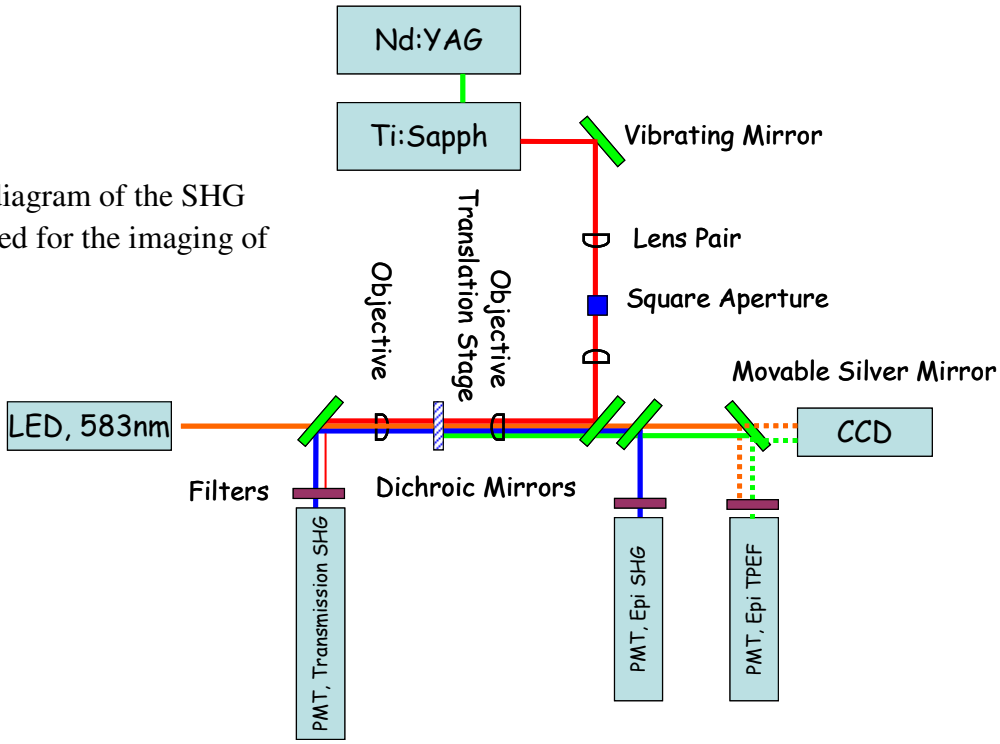

Figure S3. A diagram of the SHG microscope used for the imaging of GFP.

IV. Expression of His_8-GFP

Materials

The his_8-GFPuv pT7-7 plasmid was a generous gift from Dinesh Yernool, Purdue University.

Expression of His_8-GFPuv

The his_8-GFPuv plasmid (50 µg) was transformed into 50 µL XL1-blue cells (Invitrogen), which were incubated on ice for 30 minutes. The cells were heat-shocked at 42°C for 45 s, cooled on ice for 2 min, then added to 1 mL 2xYT media and incubated at 37°C for 1 h. The cells were collected by centrifugation at 14000 rpm for 5 minutes and the cell pellet was resuspended in 200 µL 2xYT media. The cells were plated on agar plates treated with 100 µg/mL ampicillin and incubated at 37°C overnight. One colony was added to 10 mL 2xYT media treated with 100 µg/mL ampicillin and incubated with shaking at 37°C for 4 h. The plasmid was extracted using the Wizard Plus SV Miniprep kit (Promega). The purity of the DNA was checked using the Abs_{260}/Abs_{280} ratio after extraction. The plasmid was transformed into BL21(DE3) cells (Invitrogen) by adding 1 µL of the plasmid to 50 µL cells and incubating on ice for 30 min. The cells were heat-shocked at 42°C for 45 s, cooled on ice for 2 min, then resuspended in 1 mL 2xYT media. The cells were shaken at 37°C for 1 h and collected by centrifugation. The cell pellet was resuspended in 1 mL 2xYT media and the cells were plated onto agar plates treated with 100 µg/mL ampicillin. The plates were incubated at 37°C for 12 h. One colony was added to 10 mL 2xYT media treated with 100 µg/mL ampicillin and were shaken at 37°C until the OD_{600} reached 0.8. Next 1 mL of the 10 mL culture was added to 1L of 2xYT treated with 100 µg/mL ampicillin. The cells were shaken at 37 °C until the OD_{600} reached 0.5-0.8. The cells were induced using 1 mM isopropyl-β-D-thiogalctopyranoside and shaken at 37 °C until the OD_{600} reached 1.6. The cells were collected by centrifugation at 13,500 rpm for 10 min. The cell pellets were checked for green fluorescence using a hand-held UV lamp before proceeding. The cell pellets were combined and resuspended in 50 mL binding buffer for purification (10 mM imidazole, 300 mM NaCl, 50 mM NaH_2PO_4, pH 8.0). The cells were French pressed until the solution was homogeneous and collected by centrifugation at 18000 g for 45 min. The supernatant was filtered through 0.2 µm membrane filters and loaded onto a HisTrap HP column (GE Life Sciences) at 4°C using an AKTA Prime fast performance liquid chromatography system (GE Life Sciences) for purification. Immediately before purification the binding and elution buffer (250 mM imidazole, 300mM NaCl, 50 mM NaH_2PO_4, pH 8.0) were treated with 1 mM PMSF (phenylmethanesulfonylfluoride) and 0.5 mM DTT (dithiothreitol). The protein was eluted using 250 mM imidazole and the fractions containing the protein were pooled. The pooled fractions were dialyzed twice using regenerated cellulose membranes (12 kDa cutoff, Spectra/Por) against phosphate buffered saline, pH 7.4. The fractions were characterized using 12.5 % acrylamide SDS-PAGE gel electrophoresis and Western blot analysis. For Western blot analysis the SDS-PAGE gels were transferred onto nitrocellulose membranes on ice for 1.5 h at 100V. A Ponceau S stain was used to confirm the transfer of protein onto the membrane. The membranes were rinsed three times with tris-buffered saline with 1% Tween- 20 (TBS/T). The membranes were blocked with 5% milk for 1 h at room temperature, rinsed three more times with TBS/T, and treated with a 1:5000 dilution of the primary antibody, either rabbit anti-his6

IgG or rabbit anti-GFP IgG (Abcam). The membranes were rinsed three times with 0.5% milk and treated with the secondary antibody, horseradish peroxidase-anti-rabbit IgG (eBioscience) at a 1:20,000 dilution for 35 min. The membranes were rinsed three times with TBS/T and incubated with 1:1 A:B reagents (Supersignal West Pico Chemiluminescent Substrate, Pierce) for 1 min. The blots were exposed to CL-Xpose Film (Pierce) for detection for 30 s – 1 min. The final protein concentration was determined using a microBCA Protein Assay Kit (Pierce).

V*. Lysozyme Crystallization*

Lysozyme from chicken egg white was purchased from Sigma and used without further purficiation. Crystallization was performed using the batch method. Briefly, 30 mg/mL of lysozyme dissolved in a 0.1 M solution of sodium acetate buffered at pH 4.8 was added to an equal volume of a 3.5% *w/v* of NaCl solution. Crystals were allowed to grow for 24 hr, before SH measurements were taken.

References

1. Williams, R. M.; Zipfel, W. R.; Webb, W. W., Interpreting second-harmonic generation images of collagen I fibrils. *Biophys. J.* **2005,** 88, 1377-1386.
2. Moad, A. J.; Moad, C. W.; Perry, J. M.; Wampler, R. D.; Begue, N. J.; Shen, T.; Goeken, G. S.; Heiland, R.; Simpson, G., J., NLOPredict: Visualization and data analysis software for nonlinear optics. *J. Comput. Chem.* **2007,** 28, 1996-2002.
3. Kleinman, D. A., Nonlinear dielectric polarization in optical media. *Phys. Rev.* **1962,** 126, 1977-1979.
4. Dailey, C. A.; Burke, B. J.; Simpson, G. J., The General Failure of Kleinman Symmetry in Practical Nonlinear Optical Applications. *Chem. Phys. Lett.* **2004,** 390, 8-13.
5. Wampler, R. D.; Begue, N. J.; Simpson, G., J., Molecular Design Strategies for Optimizing the Nonlinear Optical Properties of Chiral Crystals. *Cryst. Growth and Design* **2008,** ASAP.